

# Electrochemical Characterization and Oxygen Reduction Kinetics of Cu-incorporated Cobalt Oxide Catalyst

Immanuel Vincent and Dmitri Bessarabov\*

DST HySA Infrastructure Centre of Competence, Faculty of Engineering, North-West University, Potchefstroom, 2520, South Africa

\*E-mail: [dmitri.bessarabov@nwu.ac.za](mailto:dmitri.bessarabov@nwu.ac.za)

Received: 13 May 2016 / Accepted: 22 June 2016 / Published: 7 August 2016

---

Electrochemical characterization of Cu incorporated cobalt oxide is carried out and oxygen reduction reaction (ORR) activity also determined at different catalyst loadings (CLs), using thin film rotating disk electrode (RDE) technology. Electrochemical properties such as the electrochemical surface area (ECSA), ORR, mass activity specific activity, as well as the durability of the electrocatalyst is evaluated. ESCA is determined by cyclic voltammetry (CV) measurements in 1 M KOH at 30 °C, using scanning rates of 5–100 mV s<sup>-1</sup>. The active CO<sub>3</sub><sup>+</sup> present in the surface of the (CuCoO)<sub>x</sub> lattice acts as a donor–acceptor in the reduction sites during the ORR. The oxygen reduction activity for (CuCoO)<sub>x</sub> catalysts is evaluated at various rotation rate in the range 400–3000 rpm. The data are analysed using the Koutecky–Levich relationship; parallel lines indicate first-order kinetics. The number of electrons transfer favours a 4e<sup>-</sup> pathway oxygen reduction process, the rate constant of the reaction is in the range 0.07–0.11 mol L<sup>-1</sup> s<sup>-1</sup> at CL 0.05 mg cm<sup>-2</sup>.

---

**Keywords:** (CuCoO)<sub>x</sub>, Electrochemical surface area, Oxygen reduction reaction, Koutecky–Levich relationship

## 1. INTRODUCTION

The oxygen evolution (OER) and oxygen reduction reaction (ORR) are the primary reactions in fuel cells and electrolyzers. The efficiency of these reactions is depend on the electrocatalysts of both the reactions. Conventionally, the noble metal catalyst such as IrO<sub>2</sub> and Pt have been typically used in conventional OER and ORR electrocatalyst in fuel cell and electrolyzers [4,5,6]. However, platinum is very expensive and iridium is one of the poorly available material in Earth crust. The combination of these factors maintains high cost of fuel cell and electrolysis technologies.

Recently, several exciting non-precious-metal OER and ORR catalysts have been identified as having activity comparable to that of Pt [7,8]; however, their stability still needs to be proven. Low

cost and freely available materials such as manganese (Mn), nickel (Ni) and cobalt (Co) have recently investigated because their electrocatalytic activities towards the ORR are comparable to those of noble-metal-based electrocatalysts [9–13]. Among these electrocatalysts, spinel cobaltite oxides (such as  $\text{Co}_3\text{O}_4$ ) have attracted much attention because of their abundance and ease of accessibility. The cobalt oxide, surprisingly acts as a bi-functional catalyst, so it can be used in both the OER and ORR under alkaline conditions when coupled with carbon supports [13]. The  $\text{Co}^{2+}$  at the tetrahedral sites and  $\text{Co}^{3+}$  at the octahedral sites provide promising activity and stability under alkaline conditions [14–16]. Furthermore, theoretical simulations and experimental evidence have shown that the ORR activity is strongly correlated to the morphology and electronic structure of the  $(\text{CoO})_x$  [17].

The copper ion was introduced into the  $(\text{CoO})_x$  lattice via doping to reduce the overpotential and increases the activity [10,17–20]. The existence of Cu at the cobalt oxide surface octahedral sites plays a favourable role for the OER. The increased activity for OER with these  $\text{CuCo}_3\text{O}_4$  materials is due to the beneficial partial replacement of cobalt ions by copper ions in the  $\text{Co}_3\text{O}_4$  structure. This partial replacement of the cobalt ion by the copper ion decrease the electrical resistivity [22]. The OER characterises of the  $(\text{CuCoO})_x$  have been investigated over past decade [21][24]. However, little research has been done on Cu-incorporated Co-based catalysts for electrolysis [13]. One of the major drawbacks of this catalyst requires higher catalyst loading on the electrode surface which hinder the usage of this catalyst in both the fuel cell and electrolyser. So, a detailed study required to understand the relation between catalyst loading and its activity. In addition, the electron transfer (n) mechanism and the rate constant also inevitable to strength the investigation.

The aim of the present study is to characterize the catalytic activity and electrochemical properties of the Cu-incorporated Co catalyst, with different catalyst loadings (CLs), for ORR. Specific objectives were the following: thin film coating on the surface of the electrode, recording of cyclic voltammograms of  $(\text{CuCoO})_x$ ; determination of electrochemical surface area (ECSA), mass activity and specific activity; determination of number of electrons transferred and heterogeneous reaction rate constant; examination of the durability of the electrocatalysts.

We made use of a commercially available  $(\text{CuCoO})_x$  (Acta 3030; Acta SpA, Italy) for the electrochemical characterization. The electrocatalytic activity was examined by cyclic voltammetry (CV) in an inert atmosphere. Thin film RDE measurements of the ORR in an  $\text{O}_2$ -saturated electrolyte were performed at different rotation rates. The results were normalized to the amount of catalyst on the electrode and the surface area of the electrode in order to calculate the catalyst mass and specific activities, which are the accepted measures of true ORR catalytic activity. Koutecky–Levich (KL) analysis of data obtained from RDE experiments was also performed in order to determine the kinetic parameters of the ORR number of electrons transferred and the heterogeneous rate constant.

## 2. EXPERIMENTAL

### 2.1. Catalyst ink formulation

The stock solution was prepared by mixing of 20 ml of 20 % of isopropanol, 79.6 ml of ultrapure water ( $18.2 \text{ M}\Omega\cdot\text{cm}$ ) (DI; Pure lab, Elga, USA) and 0.4 mL of 20 wt% Nafion ionomer solution (1100, Ion Power Inc., USA) in a 100 mL volumetric flask. A specified quantity of the

catalyst measured in 10 ml vial and 5 ml of stock solution was added. The mixture was sonicated for 60 minutes in water bath.

## 2.2. Film coating

The working glassy carbon electrode was polished by using alumina abrasive 0.05  $\mu\text{m}$  (Allied High Tech Product Inc., USA) on microfiber polishing cloth (Buehler, USA). After, well-polished the electrode was cleaned by the ultrapure water. The cleaned electrode was placed on the specially mounted screwed gauge for catalyst dropping. A 10  $\mu\text{L}$  of catalyst mixture was dropped on the glassy carbon electrode by using digital micro pipet (multipette Xstream, Eppendorf). The film was fully covered on the electrode but not the Teflon. The film kept for overnight without any disturbance for drying. The coating of the catalyst must be uniform to avoid noisy voltammograms. Also, the stickiness of the catalyst coating on the glassy carbon was ensured to avoid the interference of the glassy carbon in both the reduction and decomposition reactions.

## 2.3. Electrochemical measurements

The cyclic voltammetry, RDE and chronoamperometry (CA) experiments were conducted by using three electrode jacketed Dr. Bob cell (Pine Research Instrumentation, USA). The catalyst coated glassy carbon (diameter: 5 mm) was acting as working electrode (WE). The reference electrode (RE) was an in-house constructed Ag/AgCl electrode and the high surface area Pt gauze was working as counter electrode. All electrochemical characterizations were carried out using a potentiostat (Biologic SP-150, Biologic, USA) and RDE (Pine Research Instrumentation) set-up.

The 1 M KOH electrolyte was filled in the Dr. Bob cell and deoxygenated by the UHP  $\text{N}_2$  for 30 min. During this time the cell temperature was equilibrated to 30°C. The catalyst coated glassy carbon electrode fixed on the rotating shaft and introduced into the electrolyte. The inserted electrodes must be in equal height in the 1 M KOH solution to reduce the resistance. The gas bubbles on the electrode surface was cleared by rotating the WE by more than 2500 rpm. All electrodes were connected to the potentiostat using appropriate shielded cables.

## 2.4. Working conditions

The surface of WE was cleaned electrochemically before the cyclic voltammetry and ORR experiments. The  $(\text{CuCoO})_x$  coated WE was cycled between 0 and 0.6 V versus Ag/AgCl for 40 cycles at 200  $\text{mV s}^{-1}$  and 20 cycles at 100  $\text{mV s}^{-1}$ . After, ending the CV measurement the KOH solution saturated by  $\text{O}_2$  for 30 minute. Then the RDE set up switched on and the rotation rate was regulated at 1600 rpm for ORR. For Kendecky- Levich analysis the ORR curves were derived by different rotation rate such as 400, 900, 1600, 2000, 2500 and 3000 rpm. In the same way, the chronoamperometric experiments were conducted at 1600 rpm to evaluate stability of the catalyst. The electrolyte solution was purged with  $\text{N}_2$  for 30 minutes prior to electrochemical measurements.

Chronoamperometry was performed at the potential 500 mV and measuring the current (mA) response as a function of time. All experiments were conducted at 30 °C.

### 3. RESULTS AND DISCUSSION

#### 3.1. Cyclic voltammetry

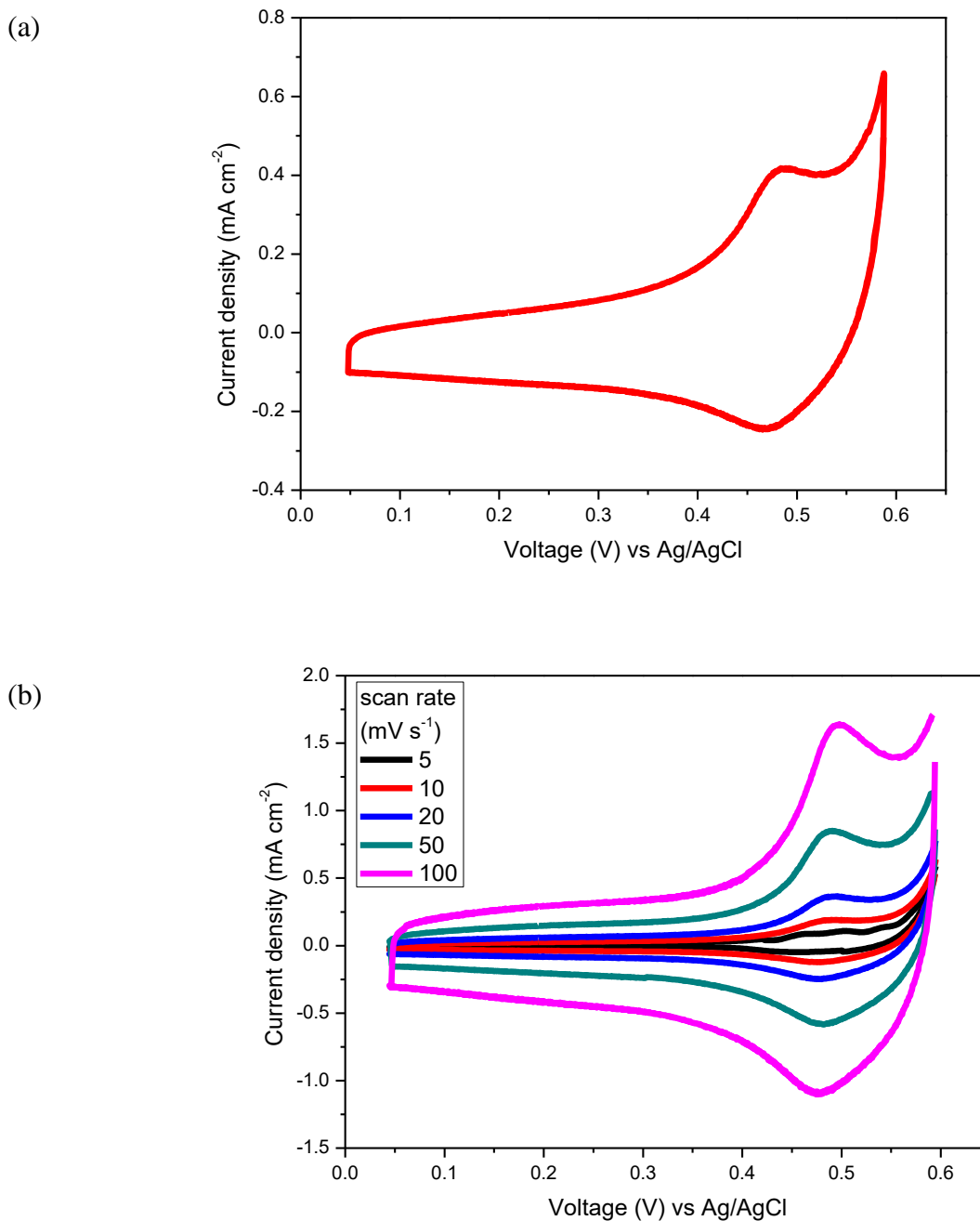


**Figure 1.** Cyclic voltammogram of 0.05 mg cm<sup>-2</sup> (CuCoO)<sub>x</sub> recorded in N<sub>2</sub>-saturated 1 M KOH at 30 °C at a scanning rate of (a) 20 mV s<sup>-1</sup>; (b) (5–100 mV s<sup>-1</sup>).

Fig. 1(a) shows the cyclic voltammetric response of  $0.05 \text{ mg cm}^{-2}$  of  $(\text{CuCoO})_x$  in  $1 \text{ M KOH}$  at  $20 \text{ mV s}^{-1}$ . The CV experiment was carried out in the potential range  $0\text{--}0.6 \text{ V}$  in positive scan mode and the voltammogram shown here is after 10 cycles. The presence of the active  $\text{Co}_3^+/\text{Co}_4^+$  in the catalyst surface was confirmed by CV [25,27]. The species  $\text{Co}_3^+$  started to oxidise on the surface of the  $(\text{CuCoO})_x$  and the current density gradually increased with the applied potential. At around potential  $0.52 \text{ V}$ , the current density sharply increased providing a perfect anodic peak. It represented the oxidation of the  $\text{Co}_4^+$  to  $\text{Co}_3^+$  [19][27]. In the reverse scan of cathodic sweep the  $\text{Co}_3^+$  was reduced to  $\text{Co}_4^+$  at  $0.48 \text{ V}$  [29]. The following reaction takes place (predictably) during the ORR and OER [27]:

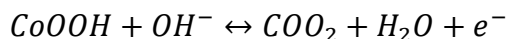
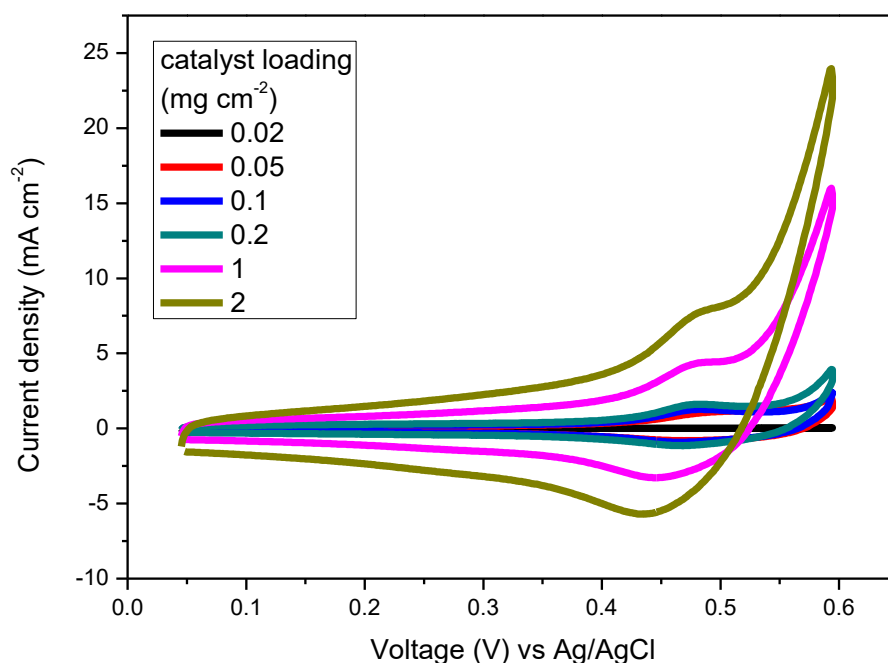
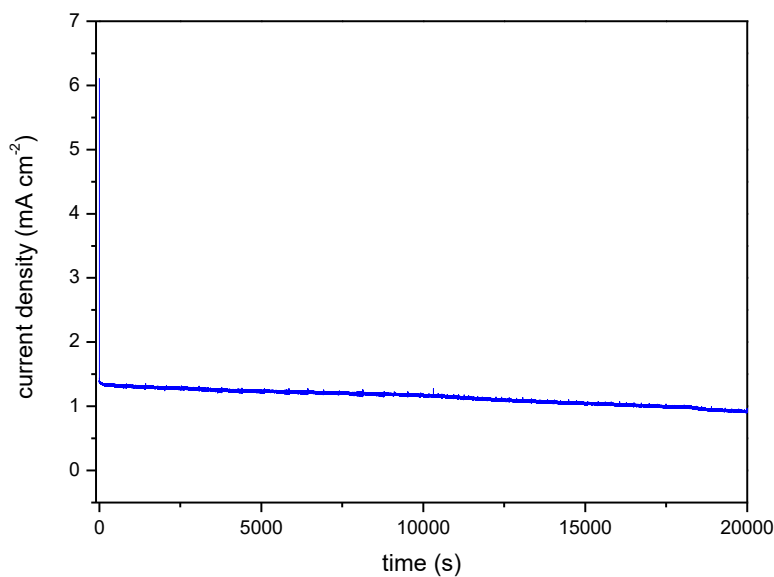


Fig. 1(b) shows the results of using different scan rates, between  $5$  and  $100 \text{ mV s}^{-1}$ . The increasing current density with increasing scan rate reveals sluggish kinetics of the system. The cobalt oxide surface consists of active  $\text{Co}_3^+$ , where the reduction occurs, and it has the capability to attract and donate electrons. During the ORR, the active  $\text{Co}_3^+$  acts as donor–acceptor at the reduction sites [30]. Fig. 2 shows the cyclic voltammetric responses when using different CLs, in the range  $0.02\text{--}2 \text{ mg cm}^{-2}$ . The charges for the CLs  $0.02$  and  $0.2 \text{ mg cm}^{-2}$  increased from  $14.08$  and  $17.36 \text{ mF}$  at  $20 \text{ mV s}^{-1}$ . This result suggests that the low CL provides a better performance. However, this is yet to be proven by ORR characteristics.



**Figure 2.** Cyclic voltammograms of  $(\text{CuCoO})_x$  with different catalyst loadings recorded in  $\text{N}_2$ -saturated  $1 \text{ M KOH}$  at  $30 \text{ }^\circ\text{C}$  at scanning rate  $20 \text{ mV s}^{-1}$ .

The durability of the catalyst film under alkaline conditions was examined by a chronoamperometry experiment. Fig. 3 shows the chronoamperometric response of  $(\text{CuCoO})_x$  catalysts in 1 M KOH at 0.5 V vs Ag/AgCL for 6 hours.



**Figure 3.** Chronoamperograms recorded at 0.5V vs Ag/AgCl for 0.1 mg cm<sup>-2</sup>  $(\text{CuCoO})_x$  in 1 M KOH.

### 3.2. Oxygen reduction characteristics

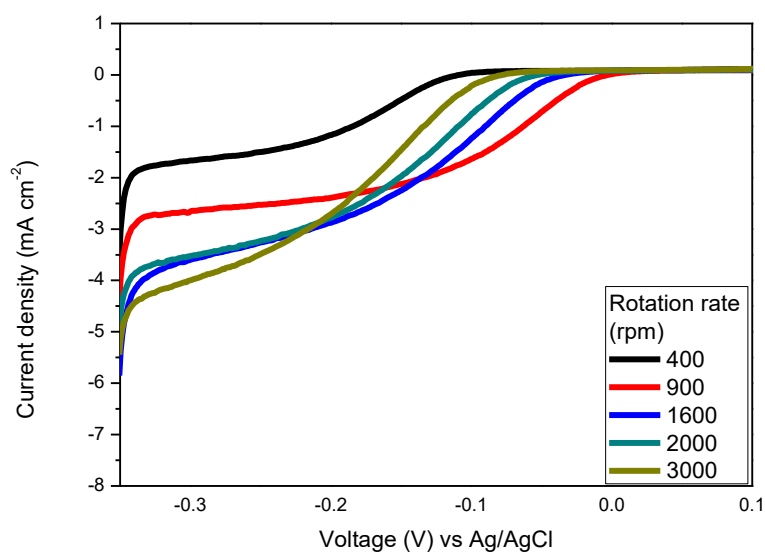


**Figure 4.** ORR polarization curves recorded for a  $(\text{CuCoO})_x$  at different electrode rotation rates: catalyst loading was 0.05 mg cm<sup>-2</sup>

The catalysts showed slow current decay approaching the limiting current density until 10000 s the corresponding decay was 12 %. After 10000 s the decay was slightly increases until 20000 s which was 17 %. The results indicate that the catalyst was moderately stable in alkaline condition.

The ORR activity experiments were carried out using linear sweep voltammetry (LSV) (1.0 M KOH solution saturated with pure oxygen, 30 min). Polarization curves for the cobalt oxide catalysts were obtained the range between  $-0.4$  and  $0.1$  V. Fig. 4 shows the LSV curves for CLs 0.05. The ORR curves appear in the diffusion-control region until  $-0.2$  V, then move to the mixed kinetic–diffusion control region from  $-0.2$  to  $0$  V, then further forward to the kinetic control region. In the diffusion-controlled region, the value of the ORR current density for the catalyst increased with increasing rotation speed.

### 3.3. Calculation of ECSA, roughness factor, mass activity and specific activity

The ECSA, roughness factor (RF), mass activity and specific activity were calculated from the following equations.

Electrochemical surface area:

ECSA of the catalyst is calculated from the electrochemical double-layer capacitances of each material using equation (1) and it is normalised with the amount of catalyst as indicated in equation (2) [31].

$$ECSA = \frac{C_{dl}}{C_s} \quad [1]$$

$$ECSA = \frac{C_{dl}}{C_s \cdot L} \quad [2]$$

In equation (2),  $C_{dl}$  is the electrochemical double-layer capacitance, determined by measuring the cyclic voltammograms at different scan rates between  $5$  and  $100$   $\text{mV s}^{-1}$  in the non-Faradaic region. The double-layer charging current is product of the scan rate and  $C_{dl}$ .  $C_s$  is the specific electrochemical double-layer capacitance of an atomically smooth surface, typically  $15\text{--}50$   $\text{mF cm}^{-2}$ . In this study, the value of  $C_s$  is  $40$   $\text{mF cm}^{-2}$  for all CLs in the  $1$  M KOH electrolyte [21].  $L$  is the loading of catalyst given in  $\text{mg cm}^{-2}$ . The RF is obtained from the ratio of ECSA to the geometric surface area ( $0.196$   $\text{cm}^2$ ) of the electrode.

$$\text{Roughness factor} = ECSA/\text{area of electrode} \quad [3]$$

Mass activity:

The electrocatalytic activity of catalysts is compared by their mass-specific and area-specific activities, using the mass-transport correction for thin-film RDEs in the following equation [31-32]:

$$J_k = (J_{lim} \times J)/(J_{lim} - J) \quad [4]$$

Where,  $J_k$  is the kinetic current density ( $\text{A/cm}^2$ ) and  $J_{lim}$  is the measured limiting current density (A). First, the ORR polarization curves are corrected by subtracting background current measured under identical conditions under a  $\text{N}_2$  atmosphere without rotation.  $J$  is the value of the curve at  $-0.1$  V and  $J_{lim}$  is the value at  $-0.3$  V versus Ag/AgCl. The mass-specific activities of the catalyst are estimated via the calculation of  $J_k$  and normalisation to the CL of the disk electrode. (For example, if  $10$   $\mu\text{L}$  of ink is loaded onto the WE and the ink contains  $5$  mg of catalyst in  $5$  mL of the ink stock

solution then the CL will be 0.01 mg.) The area-specific activities of the catalyst are calculated by normalisation to the ECSA of the catalyst using equation (3).

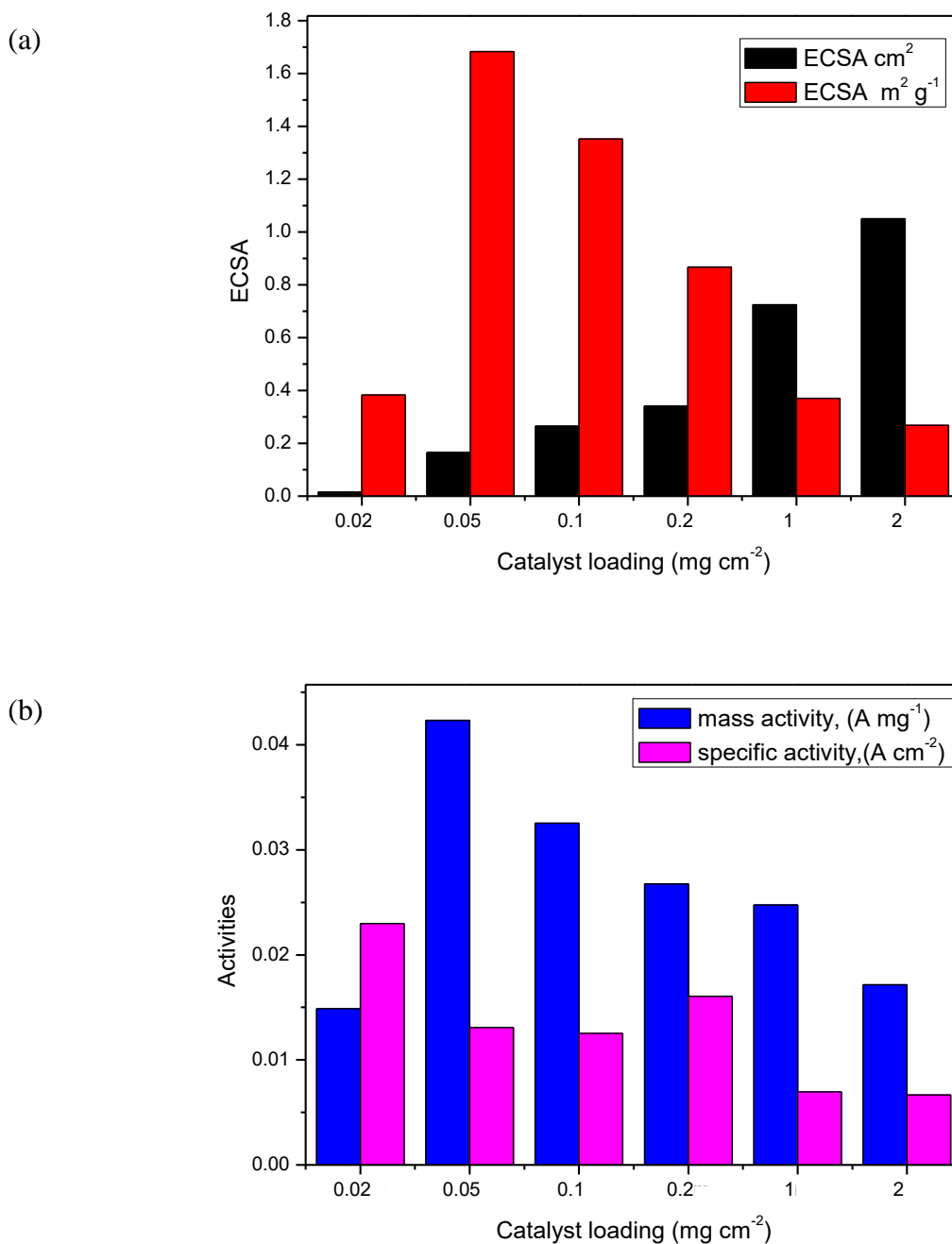


**Figure 5.** (a) Comparison of ECSA and normalized ECSA per gram of catalyst for different CLs; (b) The mass and specific activities for different CLs. All the measurements were performed in O<sub>2</sub>-saturated 1 M KOH at 30 °C (rotation rate 1600 rpm) (scanning rate 20 mV s<sup>-1</sup>).

The values of mass activity are calculated from the CL (0.05 mg cm<sup>-2</sup>) and the measured current density J (mA cm<sup>-2</sup>) at 0.3 V [32] :

$$\text{Mass activity (A mg}^{-1}\text{)} = J_k \times \frac{\text{area}}{\text{mass of catalyst}} \quad [5]$$

Specific activity:

The specific activity is calculated using the kinetic current density, the electrochemical double-layer capacitance and specific electrochemical double-layer capacitance.

$$\text{Specific activity (A cm}^{-2}\text{)} = J_k \times \text{area}/\left(\frac{C_d}{C_s}\right) \quad [6]$$

The ECSA and ORR effects were obtained for different CLs: 0.02, 0.05, 0.1, 0.2, 1 and 2 mg cm<sup>-2</sup>. Fig. 5(a) depicts ECSA values for different CLs; values for ECSA itself (in cm<sup>2</sup>) and ECSA normalized by catalyst loading (in m<sup>2</sup> g<sup>-1</sup>) were compared. The ECSA values increased with increasing CL, but the ECSA normalized by loading of catalyst values decreased with increasing CL, except in the case of the 0.02 mg cm<sup>-2</sup> CL. The reason for the low normalized ECSA of 0.02 mg cm<sup>-2</sup> was uneven coating on glassy carbon due to the insufficient catalyst. Highest normalized loading of catalyst ECSA values per gram of catalyst were found between the CL values 0.05 and 0.1 mg cm<sup>-2</sup>.

The ORR activities such as mass activity and specific activity are compared in Fig. 5(b). The mass activity between CLs 0.05 and 2 mg cm<sup>-2</sup> decreased slightly, from 0.04 to 0.017 A mg<sup>-1</sup>. The mass activities at CLs 0.05 and 0.1 mg cm<sup>-2</sup> were 0.04 and 0.032 A mg<sup>-1</sup> the reduction was 20%. The specific activities were found in the range 0.02–0.006 A cm<sup>-2</sup> for CLs 0.02–2 mg cm<sup>-2</sup>. At CL 0.02 mg cm<sup>-2</sup>, the specific activity is high, 0.05–0.2 mg cm<sup>-2</sup> it remains constant, where after it decreases. Results of these studies indicate that ECSA, and the mass and specific activities decrease as the CL increases. The high CL may increase the electron density of the surface Co<sub>3</sub><sup>+</sup> species on the (CuCoO)<sub>x</sub> electrode, which will enhance the ORR in alkaline media due to the Jahn–Teller effect in alkaline media [33]. However, the higher catalyst loading leads to higher thickness, which offer higher overpotential [34]. Also, the higher CLs conforms the appearance of high resistive CuO, which increase the overpotential sharply [18].

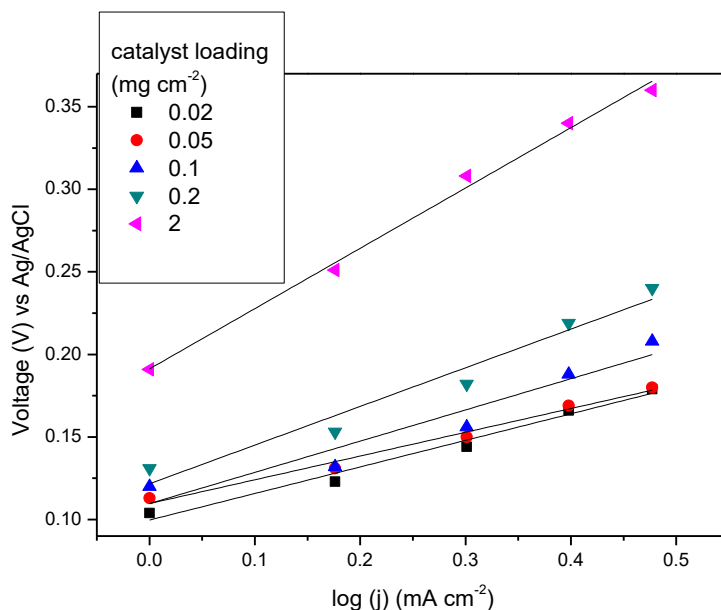


**Figure 6.** Tafel plots of ORR activity for catalysts with different catalyst loadings. All measurements were performed in O<sub>2</sub>-saturated 1 M KOH at 30 °C (rotation rate 1600 rpm).

On the other hand, the lowest CL  $0.02 \text{ mg cm}^{-2}$  leads to low ECSA and mass activity due to an insufficient amount of catalyst on the glassy carbon electrode. However, the ECSA and ORR activities are high for the CLs  $0.05$  and  $0.1 \text{ mg cm}^{-2}$ . The Tafel slopes of catalysts with the different CLs were calculated between  $0.02$  and  $2 \text{ mg cm}^{-2}$ . Fig. 6 shows the plot of  $\log J$  vs.  $V$ . The slope increases as the CL increases. The Tafel slopes for catalysts with CLs  $0.02$ – $2 \text{ mg cm}^{-2}$  were  $143$  and  $360 \text{ mV dec}^{-1}$ .

3.4 Determination of the number of electrons transferred during the ORR and the heterogeneous rate constant from Koutecky–Levic plots

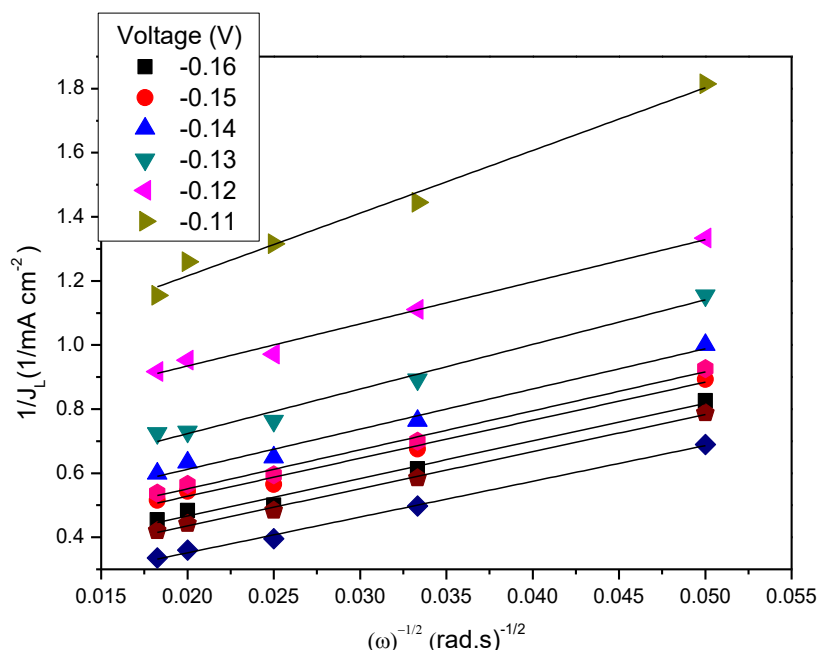


**Figure 7.** Koutecky–Levic plots at various potentials. All measurements were performed in  $\text{O}_2$ -saturated  $1 \text{ M KOH}$  at  $30 \text{ }^\circ\text{C}$  for the catalyst loading  $0.05 \text{ mg cm}^{-2}$ .

RDE studies indicate the number of electrons transferred ( $n$ ) during the ORR and the heterogeneous rate constant. The current density was measured for different voltages ranging from  $-0.2$  to  $-0.1 \text{ V}$  in the kinetic region. The inverse of the current density was plotted against the inverse of the angular velocity. The Koutecky–Levich (KL) plots ( $J^{-1}$  vs.  $\omega^{-1/2}$ ) has shown in Fig. 7 for different electrode potentials. The best linear fit slopes are shown in Fig. 7. The numbers of electrons involved in the reactions were calculated from the following KL equation (7):

$$\frac{1}{J_l} = \left( \frac{1}{0.62 \times n \times F \times A \times D^{0.67} \times \nu^{-0.16} \times C_{\text{O}_2}} \right) \times (\omega)^{-0.5} \tag{7}$$

where,  $J_l$  is the measured current density,  $\omega$  is the angular velocity ( $\text{rad s}^{-1}$ ),  $n$  is the number of electrons transferred,  $F$  is the Faraday constant ( $968500 \text{ C mol}^{-1}$ ),  $D$  is the diffusion coefficient ( $1.8 \times 10^{-5} \text{ cm}^2 \text{ s}^{-1}$ ),  $C_{\text{O}_2}$  is the bulk concentration of  $\text{O}_2$  ( $7.8 \times 10^{-7} \text{ mol cm}^{-3}$ ),  $A$  is the area of the electrode ( $0.196 \text{ cm}^2$ ),  $\nu$  is the kinematic viscosity of the electrolyte ( $1.0 \times 10^{-2} \text{ cm}^2 \text{ s}^{-1}$ ), and  $k$  is the electron-transfer rate constant ( $\text{mol L}^{-1} \text{ s}^{-1}$ ) [35].

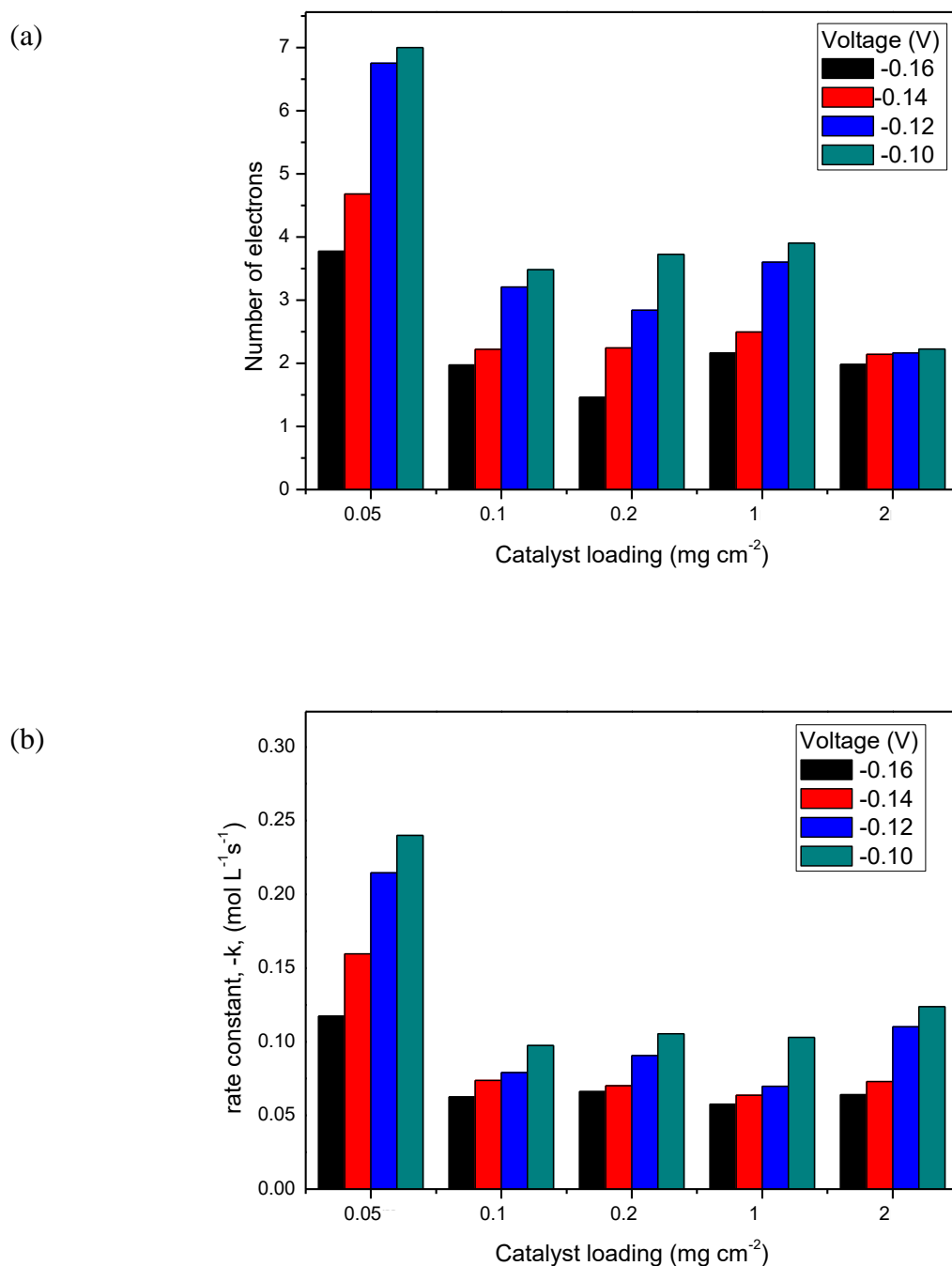


**Figure 8.** (a) Number of electrons transferred during the ORR for different catalyst loadings; (b) Rate constant during the ORR for the different catalyst loadings (rotation rate 1600 rpm).

Plots of  $J^{-1}$  versus  $\omega^{-1/2}$  at various potentials in the kinetic–diffusion region are shown in Fig. 7. Parallel lines are observed, as expected. Therefore, determination of the number of electrons transferred from the slope of the  $J^{-1}$  versus  $\omega^{-1/2}$  is expected to yield the correct result irrespective of

the kinetics of the reaction, provided that the hydrodynamic conditions remain valid. The Fig. 7 shows that the oxygen reduction current increases with increasing rotation speed.

Fig. 8(a) shows the number of electrons transferred for different CLs (rotation rate 1600 rpm). For CL  $0.05 \text{ mg cm}^{-2}$ , the number of electrons transferred ( $n$ ) is calculated to be 2–3.9 in the voltage range  $-0.16$  to  $-0.1 \text{ V}$  (at 1600 rpm) from the slopes of the KL plots. At more positive potentials, the ( $n$ ) value gradually increases; this is an indication of the formation of Hydrogen in that potential range. The number of electrons decreases with increasing rotation speed. At higher CLs the number of electrons are significantly lower; 1.5–2.5 in the voltage range  $-0.16$  to  $-0.1 \text{ V}$  (at 1600 rpm). This suggests that the catalytic mechanism operates under combined  $4e^-$  and  $2e^-$  ORR processes; the high potential favours a  $4e^-$  oxygen reduction process and lower potential supports a  $2e^-$  reduction process. The number of electrons at CL  $0.05 \text{ mg cm}^{-2}$  is higher than for other CLs; the number is the same for the 0.1, 0.2 and 1 CLs, and lowest at CL  $2 \text{ mg cm}^{-2}$ . This indicates that a thicker catalyst layer offers high resistance which is not favor to electron transfer however, this aspect requires further investigation.

The electrochemical rate constant indicate the electrocatalytic activity of the ORR. Therefore, when electrode surfaces are coated with catalyst, the respective rate constants are expected to reflect differences in the intrinsic electrocatalytic activity of the catalyst particles. The kinetic currents are obtained from the intercepts in Fig. 7. The electrochemical rate constant reflects the value of the heterogeneous activity of the electrode.

$$\frac{1}{I_l} = \left( \frac{1}{0.62 \times n \times F \times A \times D^{0.67} \times \nu^{-0.16} \times C_{O_2}} \right) \times (\omega)^{-0.5} + (1/(n \times F \times k_h \times A \times C_{O_2})) \quad [8]$$

According to equation (8), a linear relationship is expected between  $J^{-1}$  and  $\omega^{-1/2}$  when the reactions involved in the ORR are first order. The reasonably parallel lines between  $J^{-1}$  and  $\omega^{-1/2}$  represent first-order dependence of the kinetics of direct reduction in the ORR. Using equation (8), the apparent reaction rate constants ( $k_h$ ) are determined from the slopes and the intercepts of the lines of Fig. 7. The ( $n$ ) was obtained from equation (7), used for the determination of rate constant in equation (8). Fig. 7 shows that the  $J^{-1}$  and  $\omega^{-1/2}$  plots are linear at different electrode potentials, suggesting that the reactions on the electrode surface are first order [36].

A summary of the results obtained for the determination of heterogeneous reaction rate constant, for different CLs, is presented in Fig. 8(b). The values of  $k_h$  are less than unity at potentials between  $-0.16$  and  $-0.1 \text{ V}$ . For the potential range  $-0.16$  to  $-0.11$ , the rate constant was in the range  $0.063$ – $0.068 \text{ mol L}^{-1} \text{ s}^{-1}$ . The increase in the rate constant from  $-0.16$  to  $-0.10$  was only 3%. The rotation rate had no significant effect on the rate constant. The rate constant at CL  $0.05 \text{ mg cm}^{-2}$  is higher than  $0.1 \text{ mg cm}^{-2}$ . Further, increase in CL has no effect on rate constant it remains the same for all the voltages.

#### 4. CONCLUSION

In summary, we have reported on the electrochemical characterization and the oxygen reduction reaction activity of  $(\text{CuCoO})_x$  for different catalyst loadings. Along with, the electrochemical

surface area, mass activity and specific activity of Cu-incorporated cobalt oxide catalysts are also reported. The mass activity and specific activity are high in the catalyst loading range 0.05–0.1 mg cm<sup>-2</sup>. The Koutecky–Levich plot is a straight line, which indicates first-order rate kinetics. The 2e<sup>-</sup> pathway electron transfer is more predominant than 4e<sup>-</sup> at lower catalyst loading. The catalyst is moderately stable in alkaline condition. The reaction rate constant is high at 0.05 mg cm<sup>-2</sup>. The results indicate further detailed study is needed between the catalyst loading and the performance of the Fuel Cell or electrolyzers.

#### ACKNOWLEDGEMENT

Financial support from the Department of Science and Technology, South Africa, through HySA KP5 programme is gratefully acknowledged. We thank Dr. Andries Krüger for his valuable support during the initial phase of research.

#### References

1. J.D. Holladay, J. Hu, D.L. King and Y. Wang, *Catal. Today*, 139 (2009) 244.
2. M. Carmo, D.L. Fritz, J. Mergel and D. Stolten, *Int. J. Hydrogen Energy*, 38 (2013) 4901.
3. C.C. Pavel, F. Cecconi, C. Emiliani, S. Santuccioli, A. Scaffidi and S. Catanorchi, *Angew. Chem. Int. Ed. Engl.*, 53 (2014) 1378.
4. Y. Leng, G. Chen, A.J. Mendoza, T.B. Tighe, M. a Hickner and C.Y. Wang, *J. Am. Chem. Soc.*, 134 (2012) 9054.
5. F.A. Frame, T.K. Townsend, R.L. Chamousis, E.M. Sabio, T. Dittrich and N.D. Browning, *J. Am. Chem. Soc.*, 133 (2011) 7264.
6. A. Mills, P.A. Duckmanton and J. Reglinski, *Chem. Commun. (Camb.)*, 46 (2010) 2397.
7. M. Lefèvre, E. Proietti, F. Jaouen and J.P. Dodelet, *Scienc.*, 324 (2009) 71.
8. G. Wu, C.M. Johnston, N.H. Mack, K. Artyushkova, M. Ferrandon and M. Nelson, *J. Mater. Chem.*, 21 (2011) 11392.
9. L. Batteries, R. Wu, X. Qian, K. Zhou, J. Wei and J. Lou, *ACS Nano.*, (2014) 6297.
10. T. Grewe, X. Deng, C. Weidenthaler, F. Schüth and H. Tüysüz, *Chem. Mater.*, 25 (2013) 4926.
11. J. Rosen, G.S. Hutchings and F. Jiao, *J. Am. Chem. Soc.*, 135 (2013) 4516.
12. M. Ammam and E.B. Easton, *J. Power Sources*, 236 (2013) 311.
13. Y. Liang, Y. Li, H. Wang, J. Zhou, J. Wang and T. Regier, *Nat. Mater.*, 10 (2011) 780.
14. E. Fabbri, A. Haberer, K. Waltar, R. Kotz and T. Schmidt, *Catal. Sci. Technol.*, 4 (2014) 3800.
15. M. Hamdani, R.N. Singh and P. Chartier, *Int. J. Electrochem. Sci.*, 5 (2010) 556.
16. Y. Liang, Y. Li, H. Wang and H. Dai, *J. Am. Chem. Soc.*, 135 (2013) 2013.
17. Y.-X. Zhang, X. Guo, X. Zhai, Y.-M. Yan and K.N. Sun, *J. Mater. Chem. A.*, 3 (2015) 1761
18. B. Chi, H. Lin and J. Li, *Int. J. Hydrogen Energy*, 33 (2008) 4763.
19. Q. Xu, Y. Su, H. Wu, H. Cheng, Y. Guo and N. Li, *Curr Nanosci.*, (2015) 107.
20. X. Wu and K. Scott, *J. Mater. Chem.*, 21 (2011) 12344.
21. S.K. Bikkarolla and P. Papakonstantinou, *J. Power Sources*, 281 (2015) 243.
22. J. Jia, X. Li and G. Chen, *Electrochim. Acta*, (2010). 8197.
23. R. Ning, J. Tian, A.M. Asiri, A.H. Qusti, A.O. Al-Youbi and X. Sun, *Langmuir*, 29 (2013) 13146.
24. J. Wang, T. Qiu, X. Chen, Y. Lu and W. Yang, *J. Power Sources*, 268 (2014) 341.
25. B.M. Khalid Fatih, *Can. J. Chem.*, 75(11) 1597.
26. P. Stefanov, I. Avramova, D. Stoichev, N. Radic, B. Grbic and T. Marinova, *Appl. Surf. Sci.*, 245 (2005) 65.
27. J. Xu, P. Gao and T.S. Zhao, *Energy Environ. Sci.*, 5 (2012) 5333.

28. J. Landon, E. Demeter, I. Nilay, C. Keturakis, I.E. Wachs and R. Vasic, *ACS Catal.*, 2 (2012) 1793.
29. B. Lu, D. Cao, P. Wang, G. Wang and Y. Gao, *Int. J. Hydrogen Energy*, 36 (2011) 72.
30. F. Švegl, B. Orel, I. Grabec-Švegl and V. Kaučič, *Electrochim. Acta*, 45 (2000) 4359.
31. J.D. Benck, Z. Chen, L.Y. Kuritzky, A.J. Forman and T.F. Jaramillo, *ACS Catal.*, 2 (2012) 1916.
32. Y. Garsany, O. a Baturina, K.E. Swider-Lyons and S.S. Kocha, *Anal. Chem.*, 82 (2010) 6321.
33. R.G. Compton, *Comprehensive Chemical Kinetics*, Elsevier, 1987.
34. Á. Kriston, T. Xie, D. Gamliel, P. Ganesan and B.N. Popov, *J. Power Sources*, 243 (2013) 958.
35. J. Qiao, L. Xu, P. Shi, L. Zhang, R. Baker and J. Zhang, *Int. J. Electrochem. Sci.*, 8 (2013) 1189.
36. J. Masa, C. Batchelor-McAuley, W. Schuhmann and R.G. Compton, *Nano Res.*, 7 (2014) 71.

© 2016 The Authors. Published by ESG ([www.electrochemsci.org](http://www.electrochemsci.org)). This article is an open access article distributed under the terms and conditions of the Creative Commons Attribution license (<http://creativecommons.org/licenses/by/4.0/>).